Mine Water Environ (2016) 35:221–234
DOI 10.1007/s10230-015-0350-8

TECHNICAL ARTICLE

Hydrogeological Behavior of a Store-and-Release Cover: A Comparison Between Field Column Tests and Numerical Predictions With or Without Hysteresis Effects

Bruno Bossé[1,2] · Bruno Bussière[1] · Abdelkabir Maqsoud[1] · Rachid Hakkou[2,3] · Mostafa Benzaazoua[1,2]

Received: 13 December 2014 / Accepted: 13 June 2015 / Published online: 28 June 2015

Abstract Non-hysteretic numerical codes are often used to design store-and-release (SR) cover systems. Hysteretic and non-hysteretic predictions were compared using field measurements with instrumented column tests, consisting of fine-grained SR material (phosphate limestone waste) with high hysteretic behavior (hysteretic ratio ≈ 11) placed over a capillary break layer. Transient unsaturated water flow was then predicted using a one-dimensional code (HYDRUS-1D) under semi-arid climatic conditions over 1 year. Non-hysteretic simulation based on the main wetting curve of the SR material and hysteretic simulation were validated with the measured data. The compared results showed better agreement between measured and predicted values for non-hysteretic simulation during wet periods, whereas the hysteretic scenario showed better agreement with field measurements during dry periods. The influence of hysteresis effects on the complex transient unsaturated water flow of the tested scenarios and conditions is considered minor.

Keywords Numerical modeling · Phosphate limestone waste · Soil–atmosphere interactions · Unsaturated flow

Introduction

Water retention curves (WRCs) are essential inputs for simulating transient unsaturated water flow in soils. The WRC function relates the volumetric water content, θ (cm^3/cm^3), to the negative pore water pressure, ψ (i.e. matric suction—kPa) of a given material (e.g. Fredlund and Rahardjo 1993). Many authors have found that significant hysteresis effects can affect the representativeness of WRCs used in numerical predictions (e.g. Abbasi et al. 2012; Mitchell and Mayer 1998; Royer and Vachaud 1975; Šimůnek et al. 1999; Vereecken et al. 1995; Watson et al. 1975). Indeed, at a given suction value for a given material, and depending on the wetting–drying path, volumetric water content can vary significantly. Therefore, the relationship between suction and volumetric water content is not unique, but instead comprises a series of WRCs called wetting or drying scanning curves. These curves are located within a hysteresis loop bounded by a main wetting curve (MWC) and a main drying curve (MDC). The MWC is obtained by wetting a dry material, whereas the MDC is obtained by draining a fully saturated material (Davis et al. 2009; Haines 1930; Miller and Miller 1956; Mualem and Beriozkin 2009; Poulovassilis 1962). According to Maqsoud et al. (2012), the main causes of hysteresis identified in the literature are the "ink bottle" effect, the liquid–solid contact angle difference between wetting and drying processes, and the aggregate effects of mechanisms such as swelling and shrinking, air entrapment, and capillary condensation. Many theoretical and empirical models have been developed to predict or describe the hysteretic

Electronic supplementary material The online version of this article (doi:10.1007/s10230-015-0350-8) contains supplementary material, which is available to authorized users.

✉ Bruno Bussière
bruno.bussiere@uqat.ca

[1] Research Institute on Mines and the Environment, Univ du Québec en Abitibi-Témiscamingue, 445 Boul de l'Université, Rouyn-Noranda, QC J9X 5E4, Canada

[2] IDRC (Canada) Research Chair in Management and Stabilization of Mining and Industrial Wastes, Univ Cadi Ayyad, Marrakech, Morocco

[3] LCME, Faculté des Sciences et Techniques, Univ Cadi Ayyad, BP 549, 40000 Marrakech, Morocco

behavior of granular materials (e.g. Haverkamp et al. 2002; Hogarth et al. 1988; Huang et al. 2005; Kool and Parker 1987; Li 2005; Liu et al. 1995; Maqsoud et al. 2012; Mualem 1974, 1977, 1984a, b; Nimmo 1992; Nuth and Laloui 2008; Parker and Lenhard 1987; Parlange 1976; Pedroso and Williams 2010; Pham et al. 2003; Poulovassilis 1962; Scott et al. 1983; Topp 1971; Yang et al. 2012a; Zhou 2013).

Engineered cover systems based on soil–atmosphere interactions and capillary barrier effects are often used in arid or semi-arid climates to control water infiltration through landfill or mine waste disposal areas (e.g. Albright et al. 2004; Benson et al. 2002; Bossé et al. 2015; Dwyer 2003; Morris and Stormont 1997; Rock et al. 2012; Zhan et al. 2014). Capillary barrier effects occur when a fine-grained material layer is placed over a coarse-grained material (e.g., Shackelford et al. 1994; Stormont and Anderson 1999). The transient unsaturated hydrogeological behavior of this configuration allows fine-grained material to retain water during wet periods and release it to the atmosphere by evaporation (or evapotranspiration, ET) during dry periods. The engineered cover systems applied to control water infiltration are called store-and-release (SR) covers, ET covers, or water balance covers. In this study, the term SR cover is used.

To design SR covers, numerical modeling is usually used to determine the effectiveness of the SR layer thickness under natural and extreme conditions and to predict hydrogeological performance. Nevertheless, only a few studies have compared model predictions with field data for SR covers with capillary barrier effects (e.g. Fayer et al. 1992; Fayer and Gee 1997; Khire et al. 1999; Morris and Stormont 1998; Ogorzalek et al. 2008; Scanlon et al. 2002, 2005). The complex transient unsaturated flow across the SR cover was usually simulated using codes integrating soil–atmosphere interactions and non-hysteretic unsaturated water flow equations (e.g. Benson 2007; Benson et al. 2004; Dwyer 2003; Khire et al. 1997, 1999; Ogan et al. 1999; Ogorzalek et al. 2008; Scanlon et al. 2005). Indeed, the role of hysteresis effects in the hydrogeological behavior of SR covers has largely been neglected, mainly due to the difficulty of measuring the MWC of fine-grained materials and the complexity of incorporating theoretical hysteresis models into numerical codes (Khire et al. 2000; Ogorzalek et al. 2008; Scanlon et al. 2005). However, it was recently suggested to include hysteresis effects in numerical simulations for the design of engineered cover systems (e.g. Huang et al. 2011; Lee 2007; Tan et al. 2009; Yang et al. 2012b). Zhang et al. (2009) and Yang et al. (2012a) showed that predictions using hysteresis models agreed better with experimental data for a capillary barrier cover and a compacted clay cover subjected to cyclic drying and wetting (laboratory experiments). According to these authors, hysteresis models produce significantly different predictions (pore water pressure distributions, breakthrough occurrences, and percolation velocity) than non-hysteresis models, which are commonly based on the MDC.

This article assessed the influence of hysteresis effects in the WRC on the performance of SR covers exposed to semi-arid climatic conditions (Morocco). First, hysteresis effects on SR material were determined in laboratory tests. Field results from instrumented columns simulating SR covers (Bossé et al. 2013) were then compared to numerical predictions obtained with a one-dimensional code (HYDRUS-1D) that can incorporate soil–atmosphere interactions and hysteresis effects.

Methods and Characterization Results

Main Hydrogeological Properties

Previously, some of the basic hydrogeological properties of the fine- (classified as non-plastic sandy silt according to the unified soil classification system (USCS); e.g. McCarthy 2007) and coarse-grained (USCS-classified as poorly graded gravel with sand) materials, consisting respectively of phosphate limestone waste and coarse reactive tailings, were investigated (see Bossé et al. 2013). For the fine-grained material, the MDC (Supplemental Fig. 1) was obtained using a pressure chamber (Tempe cell; ASTM D6836-02 2008) and saturated salt solutions. The saturated hydraulic conductivity (k_{sat}) was determined using a rigid wall permeameter with the falling head method (adapted from ASTM D5856-95 2002). The k_{sat} value measured at a porosity of 0.43 was 5.7×10^{-6} cm/s. Supplementary wetting tests using saturated salt solutions were performed to measure the hysteretic behavior of the fine-grained material at high suction values. For the coarse-grained material, the WRC (Supplemental Fig. 1) was obtained using an instrumented column test, described below. The k_{sat} value, determined with the constant head method (ASTM D2434-68 2006) at a porosity of 0.38, was 5.9 cm/s.

Additional laboratory instrumented column tests (adapted from Yang et al. 2004) were performed to determine the WRC of the coarse-grained material and the MWC and primary scanning curves for the fine-grained material (Supplemental Fig. 1 and Fig. 1). The columns consist of a transparent acrylic cylinder (14 cm in diameter) exposed to the laboratory atmosphere with a perforated plastic plate at the bottom covered with a geotextile to minimize the loss of fine particles. Tensiometers, dielectric water potential sensors (MPS-1, Decagon), and ECH_2O moisture sensors (EC-5, Decagon) were installed as the materials were placed in the column to measure suction and volumetric

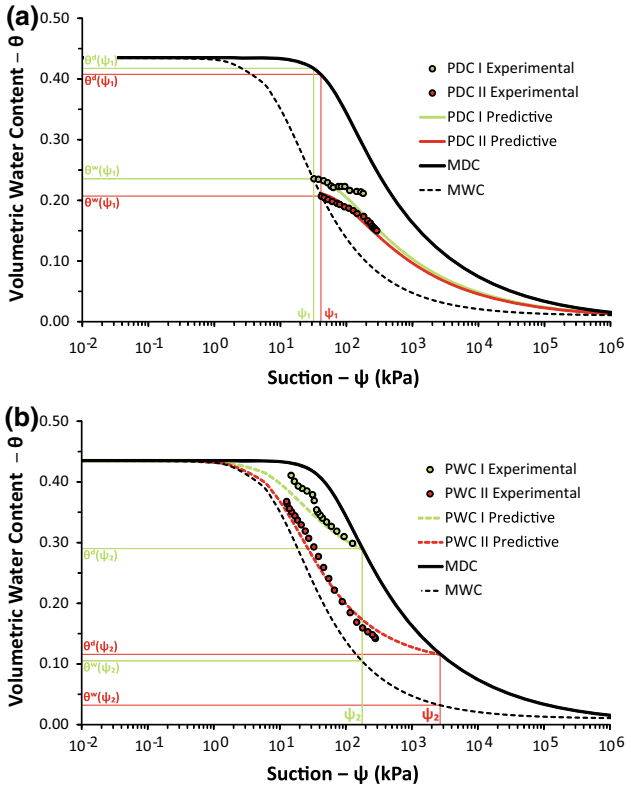

Fig. 1 Hysteresis effects in the WRC of the fine-grained material: *PDC* primary drying curves (**a**) and *PWC* primary wetting curves (**b**)

water content. The tensiometers were connected to a pressure transducer to measure matric suction (ψ) up to 90 kPa. The MPS-1 sensors measure the dielectric permittivity of porous ceramic disks, which can be related to the ψ value in the surrounding soils. The manufacturer's recommended measurement range is from 10 to 500 kPa without material-specific calibration (Decagon 2009), and the measurement accuracy is approximately ±40 %. However, recent results obtained by the authors suggest that the reliable measurement range for this sensor type is from 10 to 200 kPa (see Bossé et al. 2013). Although ψ values higher than 200 kPa are reported below, the reader should consider 200 kPa as the upper limit of precision for the MPS-1 sensor. The moisture sensors (EC-5) estimate the volumetric water content (θ) by measuring soil dielectric permittivity (Decagon 2012). Linear material-specific calibration curves were determined for these sensors to more precisely measure volumetric water content (see Bossé 2014 for more details). The EC-5 sensor was consistently placed horizontally beside a matric suction sensor (MPS-1 or tensiometer) to relate the volumetric water content to the measured matric suction. Instruments were connected to a data acquisition system (Em50, Decagon). Readings were taken at a frequency of one reading/min for wetting cycles, and at one reading/min and two readings/h for drying cycles in the coarse- and fine-grained materials, respectively.

The fine-grained material was placed into six compacted 5 cm thick lifts to obtain a target porosity of approximately 0.43. An MPS-1 sensor was installed at 10 cm from the top surface and a tensiometer was installed at 5 cm from the bottom surface. Free drainage boundary conditions were applied at the bottom of this column during wetting and drying cycles. Wetting cycles were simulated by applying a water flux (<7 ml/min) to the center of the top surface for several hours until full saturation was reached. The drying cycles lasted more than 3 months, until volumetric water content approached 0.10. For the coarse-grained material, the column consisted of a 30 cm thick gravel layer placed at a porosity of 0.38 and instrumented with a tensiometer at 15 cm from the top surface. Rainfall was simulated by water atomization (5 ml/min) at the surface of the column until full saturation was reached (the valve at the bottom was initially closed). Free drainage boundary conditions were then applied during drying cycles.

Characterization Results and Hysteresis Effects

Supplemental Fig. 1 shows the main experimental and descriptive WRCs of the fine- and coarse-grained materials, respectively, obtained from the laboratory tests. These experimental curves were parameterized with the van Genuchten model (1980) (Eq. 1).

$$S_e = \frac{\theta - \theta_r}{\theta_s - \theta_r} = \left[\frac{1}{1 + (\alpha\psi)^n}\right]^m \quad (1)$$

where S_e is the effective degree of saturation, θ_r is the residual volumetric water content, and θ_s is the saturated volumetric water content. These values were determined using the usual graphical construction procedure (e.g. Fredlund and Xing 1994). The van Genuchten parameters are α, m (= 1 − 1/n), and n. The parameters for the different tested materials are presented in Table 1.

For the coarse-grained material, the data obtained from the laboratory column tests were similar across wetting and drying cycles (Supplemental Fig. 1), whereas for the fine-grained material, the data indicated several different drying (PDC, Fig. 1a) and wetting (PWC, Fig. 1b) paths that are typical for primary scanning curves.

The primary experimental scanning curves were compared with Scott et al. (1983) predictive model, modified by Kool and Parker (1987). This model requires the two main WRCs (MWC and MDC) for predicting the primary wetting and drying scanning curves. For a closed main hysteresis loop, the following two equations describe the primary drying (Eq. 2) and wetting (Eq. 3) curves:

Table 1 Van Genuchten parameters and hydrogeological properties

	θ_r	θ_s	α (kPa^{-1})	n	m	l	R^2	k_{sat} (cm/s)
Fine material—MDC	0.01	0.43	0.011	1.43	0.301	−1.6	0.99	5.7×10^{-6}
Fine material—MWC	0.01	0.43	0.122	1.43	0.301	−1.6	0.97	5.7×10^{-6}
Coarse material	0.01	0.38	0.73	4.94	0.797	0.5	0.62	5.9

MDC main drying curve, *MWC* main wetting curve, R^2 coefficient of determination

$$\theta^{pd}(\psi_1,\psi) = \theta_r + \left[\frac{\theta^w(\psi_1)-\theta_r}{\theta^d(\psi_1)-\theta_r}\right]\left[\theta^d(\psi)-\theta_r\right] \quad (2)$$

$$\theta^{pw}(\psi_2,\psi) = \theta_s + \left[\frac{\theta^d(\psi_2)-\theta_s}{\theta^w(\psi_2)-\theta_s}\right]\left[\theta^w(\psi)-\theta_s\right] \quad (3)$$

where ψ_1 is the suction at the reversal point from the wetting to the drying process on the MWC, ψ_2 is the suction at the reversal point from the drying to the wetting process on the MDC, $\theta^w(\psi_1)$ is the volumetric water content on the MWC at ψ_1, $\theta^d(\psi_1)$ is the volumetric water content on the MDC at ψ_1, $\theta^d(\psi_2)$ is the volumetric water content on the MDC at ψ_2, and $\theta^w(\psi_2)$ is the volumetric water content on the MWC at ψ_2.

According to Kool and Parker (1987), a hysteretic ratio (α_w/α_d were α_w and α_d are the van Genuchten parameter for the wetting and drying paths, respectively) can be deduced from the main WRCs (see the parameters in Table 1). For the studied fine-grained material, this hysteretic ratio was approximately 11, higher than the ratio ($\alpha_w = 2\alpha_d$) proposed by Kool and Parker (1987) that allows neglecting the hysteresis of the unsaturated hydraulic conductivity function (see Huang et al. 2011; Si and Kachanoski 2000; Šimůnek et al. 2009). Hence, the hysteresis of the k_u function was also taken into account in the hysteretic simulations.

The unsaturated hydraulic conductivity functions of each material, which relate the hydraulic conductivity to the matric suction, were obtained from the main WRCs (Supplemental Fig. 1) and the k_{sat} values using the van Genuchten–Mualem (1980) equation (Eq. 4):

$$k_u(S_e) = k_{sat}S_e^l\left[1-\left(1-S_e^{1/m}\right)^m\right]^2 \quad (4)$$

where S_e is the effective degree of saturation (Eq. 1) and l is a pore connectivity parameter. In this study, l was fixed at 0.5 (typical value) for the coarse-grained material and at –1.6 for the fine-grained material. This l value for the fine-grained material was obtain after a calibration process and agrees with the work of Benson (2007) and Schaap and Leij (2000), who found l values approaching –2 for fine-grained soils. Supplemental Fig. 2 shows the k_u functions of the coarse- and fine-grained material.

Based on Scott et al. (1983) predictive model, and using a similar scaling transformation procedure, Vogel et al. (1996) integrated hysteresis effects into the k_u function. This model requires the two main k_u functions (Supplemental Fig. 2) to predict the primary wetting and drying functions. For a closed main hysteresis loop, the following two equations describe the primary drying (Eq. 5) and wetting (Eq. 6) unsaturated hydraulic conductivity functions:

$$k_u^{pd}(\psi_1,\psi) = \left[\frac{k_u^w(\psi_1)}{k_u^d(\psi_1)}\right]\left[k_u^d(\psi)\right] \quad (5)$$

$$k_u^{pw}(\psi_2,\psi) = k_{sat} - \left[\frac{k_u^d(\psi_2)-k_{sat}}{k_u^w(\psi_2)-k_{sat}}\right]\left[k_{sat}-k_u^w(\psi)\right] \quad (6)$$

where ψ_1 is the suction at the reversal point from the wetting to the drying process on the main wetting k_u function, ψ_2 is the suction at the reversal point from the drying to the wetting process on the main drying k_u function, $k_u^w(\psi_1)$ is the unsaturated hydraulic conductivity on the main wetting k_u function at ψ_1, $k_u^d(\psi_1)$ is the unsaturated hydraulic conductivity on the main drying k_u function at ψ_1, $k_u^d(\psi_2)$ is the unsaturated hydraulic conductivity on the main drying k_u function at ψ_2, and $k_u^w(\psi_2)$ is the unsaturated hydraulic conductivity on the main wetting k_u function at ψ_2.

Field Column Tests

Field column tests were performed to determine whether a fine-grained material (phosphate limestone waste) could be used to reclaim an abandoned mine site near Marrakech, Morocco. One instrumented column (metallic barrels 60 cm in diameter) made of 50 cm of this SR material was placed over 30 cm of a coarse-grained material (Supplemental Fig. 3) and exposed to natural semi-arid climatic conditions (aridity index = 0.21) for a period of one and a half years (for a detailed description, see Bossé et al. 2013). The coarse-grained material beneath the SR layers acted as a capillary break layer. All columns were protected by external glass wool insulation, and circular holes were drilled at the bottom to collect the leachate. The hydrogeological behavior of these columns was assessed over 1 year (2011) using local data from meteorological stations, soil moisture (EC-TM sensors, Decagon), and matric suction (MPS-1 sensors, Decagon) measurements at 10, 25, and 40 cm depths into the fine-grained material, and the following water balance equation:

$$E = P + Irr - R_0 - P_r - \Delta S \quad (7)$$

where E is actual evaporation, P is precipitation, Irr is irrigation, R_o is runoff (nil in this column experiment), P_r is percolation or deep infiltration, and ΔS is change in the water storage. The water storage component was calculated by integrating the volumetric water content profiles during the monitoring period (e.g. Stormont and Morris 1998).

The results reported in Bossé et al. (2013) and Bossé (2014) show that the SR material effectively stored and released meteoric waters for both 1D configurations (bare surface). Only sensors at 10, 25, and 40 cm depths (see Supplemental Fig. 3) were affected by the natural climatic conditions. Note that significant hysteresis in the WRC of the SR material was observed, with measurements generally closer to the predicted MWC. A numerical investigation to integrate the hysteresis effects with the soil–atmosphere interactions was then recommended to assess the performance of the SR cover and to compare measured and predicted hydrogeological behavior.

Numerical Modeling

Many numerical codes have been developed to simulate transient unsaturated water flow (e.g. UNSAT-H, HYDRUS, VADOSE/W, HELP, LEACHM, SWAP). According to an intercode comparison (Scanlon et al. 2002), codes based on the Richards Eq. (1931), obtained by combining Darcy's law and the conservation of mass equation, are more suitable for simulating the near-surface water balance. The HYDRUS-1D code uses Galerkin-type linear finite element schemes to numerically solve the Richards equation for unsaturated water flow (e.g. Šimůnek et al. 2008, 2009). Additionally, HYDRUS-1D can simulate soil–atmosphere interactions, hysteresis effects, heat and solute transport, vapor flow, and soil extraction by plants. This HYDRUS-1D software package, version 4.15 was selected for this study because it has been used to assess the performance of engineered covers (e.g. Bohnhoff et al. 2009; Fala et al. 2005; Huang et al. 2013; Ogorzalek et al. 2008), and integrates the hysteresis effects on both the WRC and the unsaturated hydraulic conductivity function (e.g. Huang et al. 2011; Šimůnek et al. 1999; Zhang et al. 2009).

Implementation of Hysteresis Effects in HYDRUS-1D

HYDRUS-1D integrates the hysteresis effects on the WRC using the modified empirical model developed by Scott et al. (1983) (Eqs. 2, 3) based on scaling transformation. The main drying and wetting curves must be determined in order to apply the model and to estimate the scanning curves from these main WRCs using a scaling factor (Šimůnek et al. 1999).

Scott et al. (1983) model was modified by Kool and Parker (1987) and Vogel et al. (1996). Kool and Parker (1987) integrated the van Genuchten–Mualem model (1980) with Scott et al. (1983) scaling approach while taking air entrapment into account. They assumed that the shape parameters of the drying and wetting scanning curves were similar to those of the main WRCs (shape similarity theory) (e.g. Mualem and Beriozkin 2009). As suggested by Kool and Parker (1987), HYDRUS-1D also assumes similarity of the shape parameters ($\theta_r^d = \theta_r^w$ and $n^d = n^w$) for both the main WRCs and $\alpha_d < \alpha_w$ (see Eqs. 3, 4). The wetting and drying scanning curves are calculated during wet and dry periods, respectively. If the θ value reaches the saturated volumetric water content, drying occurs along the MDC, and if this value reaches the residual water content, the wetting process occurs along the MWC. Using a similar scaling transformation procedure, Vogel et al. (1996) modified the model in order to integrate hysteresis effects into the k_u function using the same parameters of the main WRCs and the saturated hydraulic conductivity (for more information, see Eqs. 5, 6, and Šimůnek et al. 2009).

Initial Conditions and Numerical Parameters

In this study, numerical simulations were conducted with HYDRUS-1D to predict the hydrogeological behavior of two SR covers having a total height of 80 cm, and consisting of 50 cm of a fine-grained material overlying 30 cm of coarse-grained material, respectively. This 1D model was discretized into 171 nodes with a nodal spacing of 10 mm. However, an element thickness of 1 mm was strategically used at the top surface and at the interface of the two materials having opposing textures, where atmospheric interactions and capillary barrier effects could increase numerical difficulties due to the sharp contrast in suction at these locations. An initial matric suction profile was assigned to each node (Supplemental Fig. 4) and aligned with typical suction (for values <200 kPa) and volumetric water content profiles measured in the field on the first day of testing.

The temporal discretization consisted of a maximum and minimum time step of 24 and 2.4×10^{-5} h, respectively. Isothermal water flow was also simulated over year 2011. The numerical approach did not consider vapor flow or heat transport. Convergence and water balance were determined for each simulation.

Boundary Conditions

For all simulations, two main boundary conditions were assigned at the column top and bottom, respectively. An

upper boundary condition simulating atmospheric interactions was derived from daily meteorological data such as rainfall (Supplemental Fig. 5), net radiation, air temperature, air humidity, and wind speed. In addition, a specific boundary condition (water layer) allowed neglecting the runoff component at the top column by water accumulation during rainfall events. A free drainage boundary condition was assigned to the column bottom (e.g. Benson 2007).

The climatic data were integrated into the numerical code as input to calculate actual evaporation and water infiltration. The actual evaporation rate was estimated from an empirical relationship between the potential evaporation and the ψ value at the soil surface (Šimůnek et al. 2009). As long as this value is between 0 and a critical lower value (hCritA), the actual evaporation rate is equal to the potential evaporation rate. The potential evaporation rate (Supplemental Fig. 5) of the bare fine-grained material (phosphate limestone waste) was automatically computed by HYDRUS-1D using the Penman–Monteith equation and a specific reflection coefficient (albedo) of 0.262. In this case, the surface resistance was set to zero (no crop), and only the aerodynamic resistance was applied. If the ψ value at the soil surface is lower than hCritA, the actual evaporation rate is controlled by the rate at which the cover material can transmit water to the atmosphere (Scanlon et al. 2002). The hCritA value used in the HYDRUS-1D code was set at 10,000 kPa, with the corresponding volumetric water content at least 0.005 higher than the residual volumetric water content (Šimůnek et al. 2009). The sensitivity of the hCritA value for numerical results is discussed later.

Comparison Between Numerical Predictions and Field Data

Two numerical simulations (hysteretic and non-hysteretic) were performed from the 80 cm cover profile (Supplemental Fig. 4) and compared with field data. The non-hysteretic scenario assumed that the MWC in the numerical approach had similar shape parameters to the MDC, and the hysteretic scenario integrated hysteresis effects on the fine-grained material initiated with the MWC (with the initial condition calculated from the MWC). The numerical simulations were performed using HYDRUS-1D and the WRC parameters presented in Table 1. The MDC scenario was also simulated, but the results are not presented here because the field values consistently departed from this curve, and due to the unrealistically high ψ values predicted by the model (from 300 to 10,000 kPa) (for more information, see Bossé 2014). As in the field tests, the observation points for the one-dimensional simulations were located at 10, 25, and 40 cm depths. Figures 2 and 3 show the simulated volumetric water content (θ) and matric suction (ψ) time trends at these depths for each scenario (hysteretic and non-hysteretic). Figure 4 and Table 2 show the main predicted components (actual evaporation and water storage) of the water balance equation (see Eq. 7). In each case, predicted values are compared with field measurements.

Suction and Volumetric Water Content

Figure 2a–c show the predicted (for the hysteretic and non-hysteretic scenarios) and measured matric suction time trends at 10, 25, and 40 cm depths, respectively. Accuracy and measurement range of the matric suction sensors are also indicated (200 kPa is the upper limit of precision for the MPS-1 sensor). For the first simulation, i.e. the non-hysteretic scenario with the MWC as the WRC for the fine-grained material, ψ values are well predicted (compared with field data) at a depth of 10 cm and well correlated with rainfall events. However, at greater depth, the predicted ψ values differ increasingly from the measured data. At 25 cm and from July to November, predictions were lower than the measured matric suctions: predicted ψ values ranged from 100 to 180 kPa, whereas measured ψ values ranged from 100 to 320 kPa (>200 kPa). At 40 cm, predicted ψ values were higher than ψ values measured in the field from January to July, with a maximum difference of approximately 200 kPa. Predicted ψ values then become lower than ψ values measured from August to December, with a maximum difference of 150 kPa. This could mean that the non-hysteretic scenario underestimated the actual evaporation. For the hysteretic scenario, the predicted matric suction was consistently higher than the measured suction at all depths. At 10 cm, the suction predicted by the hysteretic scenario was overestimated throughout the year, and covered a wider range of ψ values than for the non-hysteretic scenario. From July to November, the field measurements greatly exceeded 200 kPa and were closer to the predicted ψ values for the hysteretic scenario. However, due to the low sensor precision, it is impossible to draw conclusions about the predictive capabilities for ψ values higher than 200 kPa (Bossé et al. 2013). During the wet season (from March to June), unlike the MWC predictions, the hysteresis model cannot predict the drop in suction measured with the sensors at all depths. The numerical changes from the wetting to drying scanning curves appear to influence the numerical predictions, particularly near the surface. Predicted ψ values were lower at 25 and 40 cm depths, but higher than those for the non-hysteretic scenario ($\approx$300 kPa during dry periods).

Figure 3a–c show the predicted and measured volumetric water content time trends at 10, 25, and 40 cm depths, respectively. For the two predicted scenarios

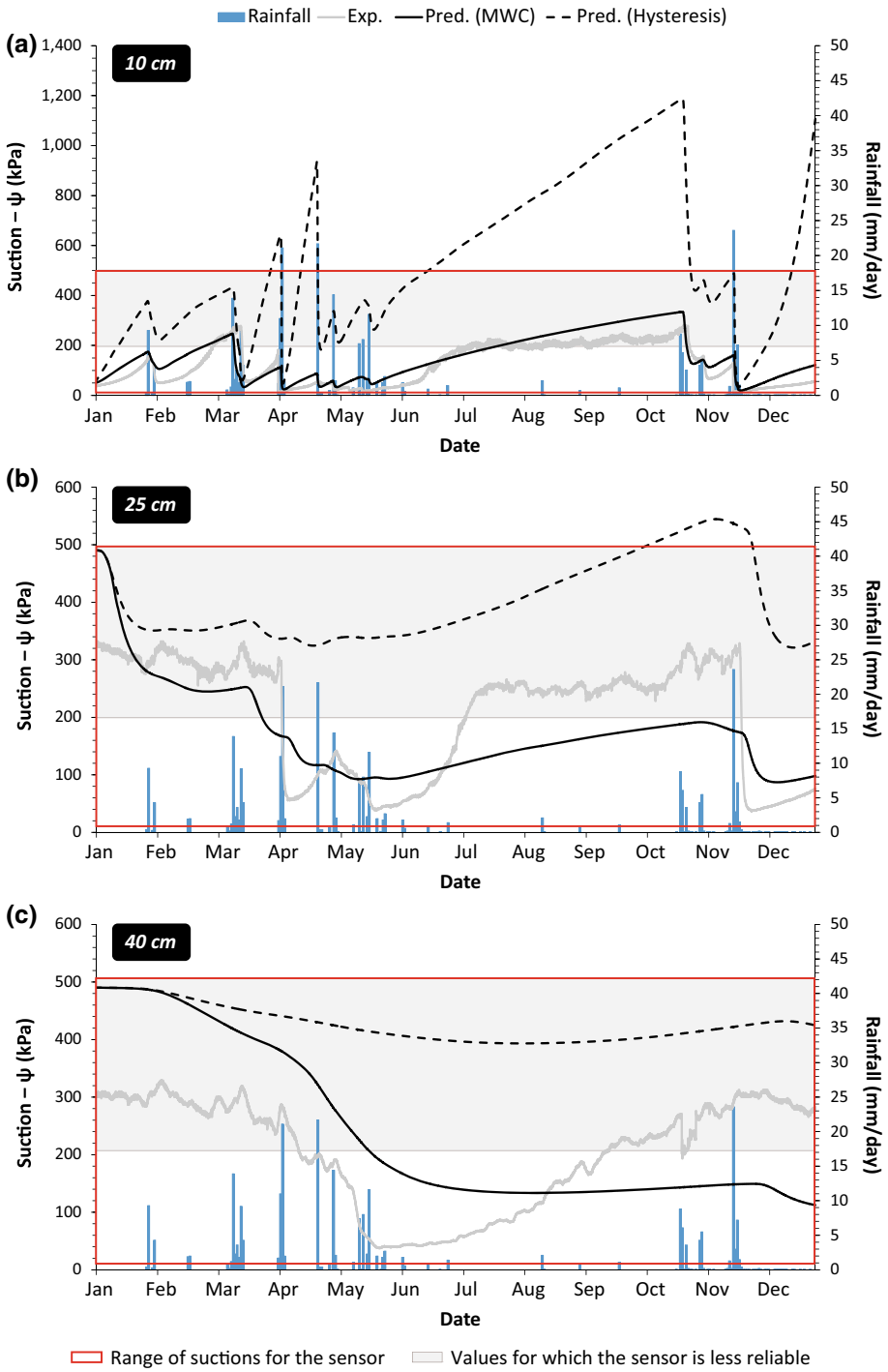

Fig. 2 Comparison between measured (*Exp.* experimental) and predicted (*Pred.*) suctions at 10 (**a**), 25 (**b**), and 40 (**c**) cm depth from the hysteretic and non-hysteretic (*MWC* main wetting curve) scenarios

(hysteretic and non-hysteretic), the magnitude of fluctuations was lower than for the field measurements. At 10 cm for the hysteretic scenario, the predicted volumetric water content (θ) time trends were underestimated, which is generally in accordance with the high predicted suctions. The θ values are also underestimated for the non-hysteretic scenario, but to a lesser extent. For both scenarios, predicted θ values ranged from 0.08 to 0.16 at 25 cm, whereas measured θ values ranged from approximately 0.06 to 0.15. At 40 cm, predicted θ values ranged from 0.08 to 0.14, whereas measured θ values ranged from 0.06 to 0.14. However, at the end of the dry season (October), when measured ψ values exceeded 200 kPa at 25 and 40 cm (values for which the matric suction sensor are less reliable), θ predictions for the hysteretic scenario were relatively close to measured values (difference <0.02). This

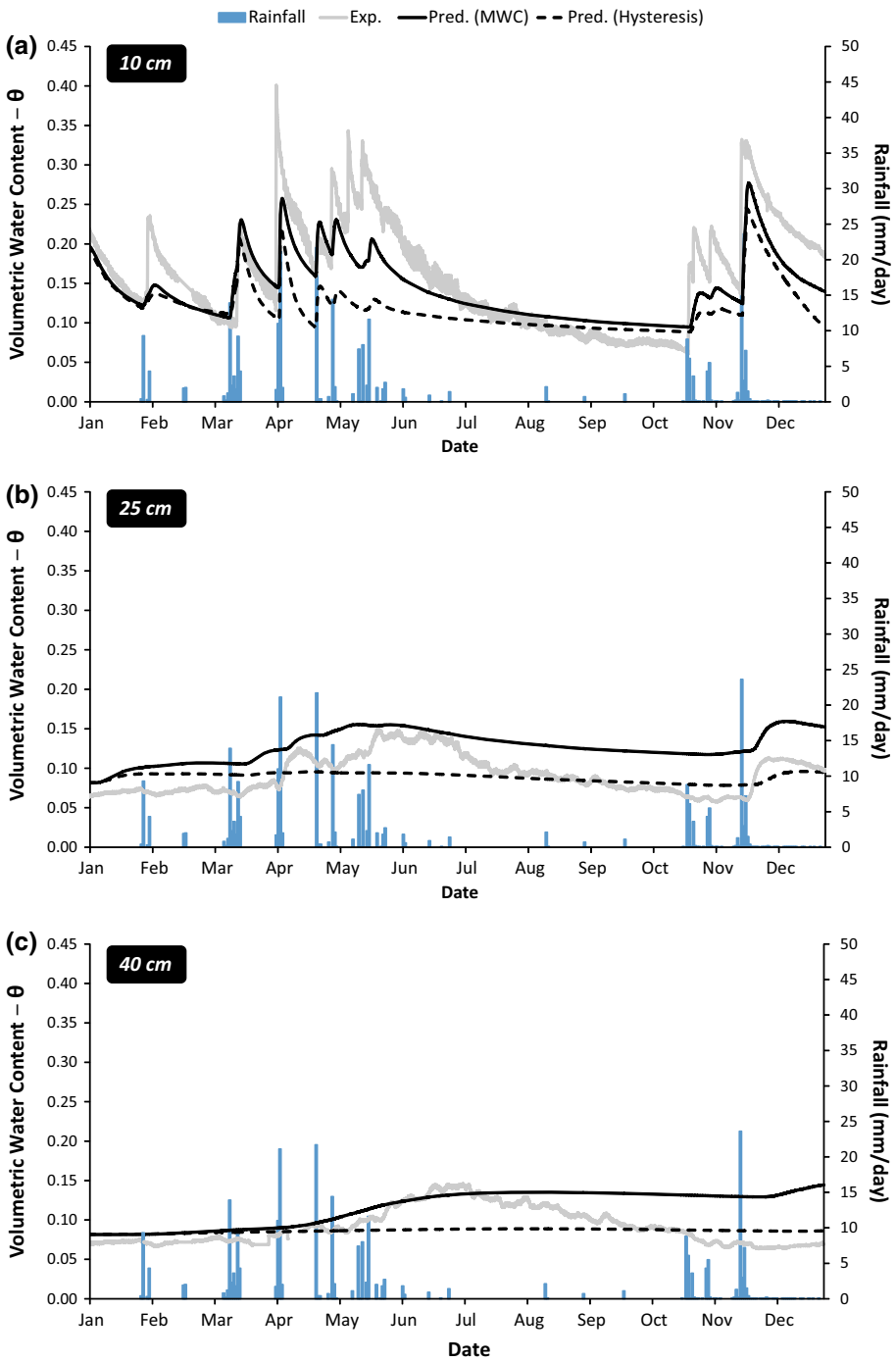

Fig. 3 Comparison between measured (*Exp.* experimental) and predicted (*Pred.*) volumetric water contents at 10 (**a**), 25 (**b**), and 40 (**c**) cm depth from the hysteretic and non-hysteretic (*MWC* main wetting curve) scenarios

supports the hypothesis that during the dry season, suctions in the soil profile are probably closer to hysteretic than MWC predictions. Additionally, the non-hysteretic scenario predicted the greatest fluctuations in the volumetric water content and slightly overestimated the θ values between the dry season and the end of the simulation. Even after rainfalls exceeding 15 mm/day, the hysteretic simulation was constant at 25 and 40 cm at approximately 0.09 volumetric water content.

Water Balance

Figure 4a, b show the simulated (for the hysteretic and non-hysteretic scenarios) and calculated (see Eq. 7) annual (year 2011) water storage and cumulative actual evaporation, respectively. These time series correlated with average daily rainfalls. For both scenarios, water storage decreased during the dry period and fluctuated during wet periods. Typically, water storage varies from 5 to 10 cm of water over the

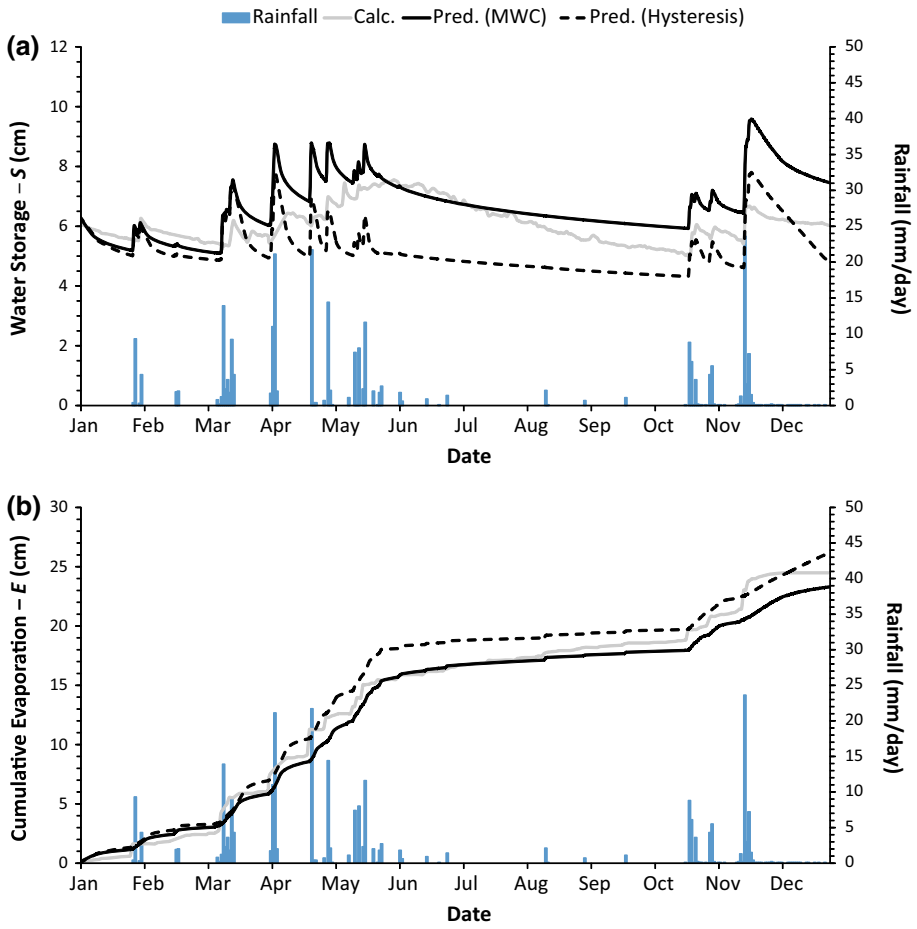

Fig. 4 Comparison between calculated (*Calc.*) and predicted (*Pred.*) water storage (**a**) and cumulative evaporation (**b**) from the hysteretic and non-hysteretic (*MWC* main wetting curve) scenarios

Table 2 Calculated and simulated water balance components (in mm) at the end of the year

	E	ΔS	S	R_o	P_r	*RMSE*—E	*RMSE*—ΔS
Calculated	246	26	0	0	0	–	–
Non-hysteretic	234	45	12	0	0	1.0	1.0
Hysteretic	261	35	−15	0	0	1.4	1.3

E cumulative actual evaporation, ΔS maximum change in water storage, S water storage at the end of the year, R_0 runoff, P_r percolation, *RMSE* root mean square error

testing period. The maximum water storage for the tested scenario was 9.6 cm (November). The greatest changes in water storage occured after rainfalls exceeding 10 mm/day. In addition, the peak magnitudes were slightly higher for the non-hysteretic scenario. Compared to the calculated water storage, the predicted values for the hysteretic scenario were slightly underestimated, particularly during the dry period (May to November). The non-hysteretic scenario water storage predictions strongly agreed with the calculated values during the first months of the year, but the predicted water storage tended to be overestimated from August until the end of the testing period. These predictions correlated with the cumulative actual evaporation time trends. Thus, Fig. 4b shows an overestimation of the cumulative actual evaporation ($\approx$20 mm) during the dry period for the hysteretic scenario, whereas the non-hysteretic scenario underestimated the cumulative actual evaporation (12 mm) at the end of the simulated year.

Table 2 presents the calculated and simulated water balance components. The accuracy of the two scenarios was determined by comparing the simulated and calculated water storage changes and cumulative actual evaporations (see Eq. 7) using the root mean square error equation (RMSE—Eq. 8).

$$RMSE = \left(\frac{1}{n}\sum_{i=1}^{n}(X_c - X_s)_i^2\right)^{0.5} \quad (8)$$

where X is the actual evaporation or water storage change, n is the number of time periods considered (350), c is the calculated value, and s is the simulated value.

As in the field, no percolation was predicted for the two scenarios. Predicted water storage changes were 45 and 35 mm, respectively, and there was a difference of $\approx$27 mm in the cumulative evaporation between the two scenarios, with the higher prediction by the hysteretic

scenario (261 mm, Table 2). Integrating the hysteresis effects into the numerical approach slightly increased the evaporation rate at the top surface. However, with RMSEs of $\approx$1.0 mm, the predicted components of the water balance equation (cumulative actual evaporation and change in water storage) in the non-hysteretic scenario were slightly closer to the calculated data.

Some conclusions can be deduced from Figs. 2, 3, and 4. For both scenarios, some differences were observed between measured and predicted values at the 10, 25, and 40 cm depths, particularly for matric suction. For example, suction values correlated better with field data for the non-hysteretic scenario at 10 cm. Note that at this depth, and from August to October ($\psi > 200$ kPa), θ values did not agree well with ψ values. Indeed, knowing that predicted matric suctions were higher than measured suctions, predicted volumetric water contents should have been lower than the measured θ values. As mentioned above, this supports the hypothesis that the matric suction sensors yielded less reliable measurements for high ψ values (>200 kPa). Note also that Bossé (2014) directly measured volumetric water content in the field at the end of the dry season and used the WRCs to estimate matric suction values. Based on those measurements, suction values of approximately 1,000 and 300 kPa were estimated at 10 and 25 cm, respectively (values closer to the hysteretic predictions, Fig. 2). Consequently, whereas predicted ψ values for the hysteretic scenario were overestimated during wet periods, predicted values for the non-hysteretic scenario could be significantly underestimated during dry seasons. In addition, the water balance predictions show that using a hysteresis or non-hysteresis model only slightly affected the simulated water balance components. Both scenarios appear to predict similar SR system behavior, with better predictions during wet and dry seasons for the non-hysteretic and hysteretic scenarios, respectively.

Sensitivity Analysis of the hCritA Parameter

A sensitivity analysis was performed to assess the influence of the critical allowed soil potential (hCritA value) on the non-hysteretic and hysteretic scenarios. Note that the influence of another parameter was also determined: the specific reflection coefficient (albedo). Because the albedo influence was negligible, it is not discussed further (see Bossé 2014 for more details).

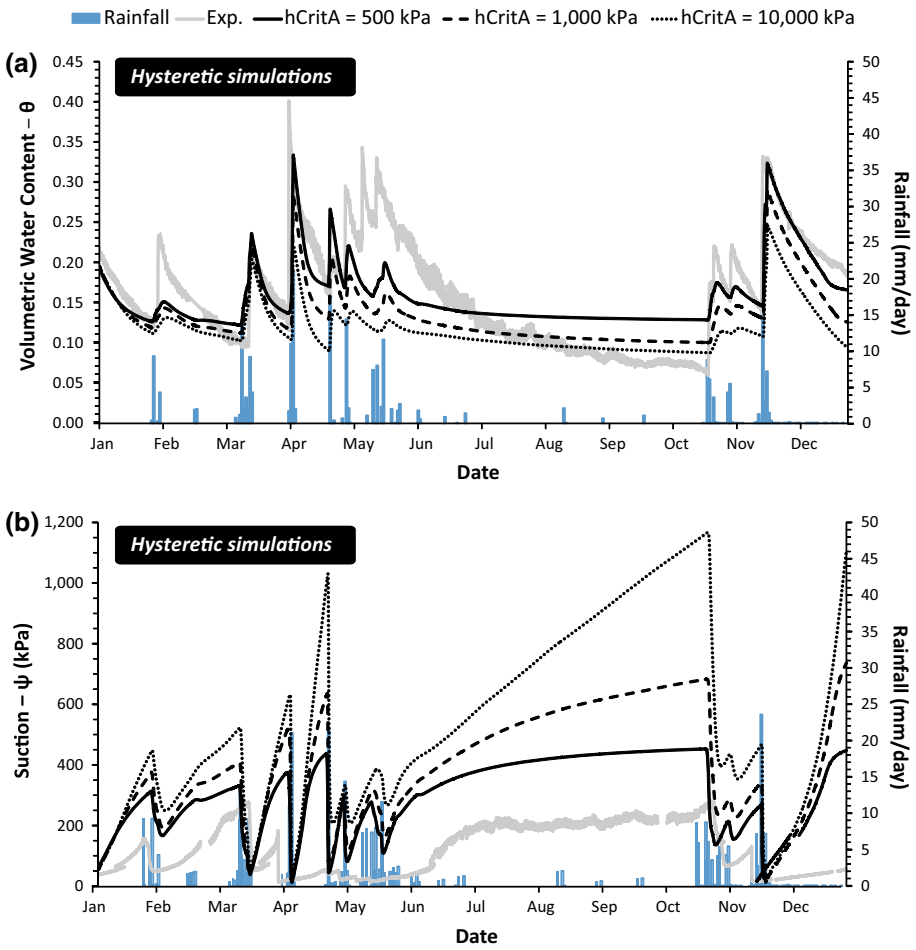

Fig. 5 Sensitivity of the hCritA value on hysteretic [volumetric water content (**a**) and matric suction (**b**) time trends] predictions at 10 cm depth

As mentioned above, the hCritA value should correspond to a ψ value close to the residual volumetric water content. An hCritA value of 10,000 kPa was used in this numerical study (based on Šimůnek et al. 2009). However, according to Pang et al. (2000), the hCritA value is usually set between 1,000 and 1,500 kPa for fine-grained materials, and at approximately 500 kPa for coarse-grained materials (e.g. sand or gravel). Wilson et al. (1997) suggested that the actual evaporation rate drops from the potential evaporation rate once the total suction at the soil surface exceeds 3,000 kPa, independently of material texture, drying time, and water content. Hence, two ψ values (500 and 1,000 kPa) were modeled and compared with the initial value (10,000 kPa) used in the previous predictions. Supplemental Fig. 6 shows the sensitivity of the hCritA value for the volumetric water content and the matric suction at 10 cm for the non-hysteretic scenario, and Fig. 5a, b show the sensitivity of the hCritA value for the hysteretic scenario. Whereas the sensitivity of the hCritA value for the non-hysteretic scenario appears low (maximum differences = 0.02 cm^3/cm^3 and 100 kPa), the hysteretic scenario indicates significant differences between the tested hCritA values. For instance, maximum differences in predictions of 0.12 cm^3/cm^3 and 700 kPa were observed after the highest rainfall events during wet periods and during the dry season (Fig. 5a, b).

In summary, for the hysteretic scenario, a lower hCritA value increased the magnitude of the θ fluctuations, decreased the ψ values, and generated predictions closer to field data during wet periods. However, a lower hCritA value can increase the pumping effects (i.e. non-closure of water retention scanning loops in simulations) in hysteretic simulations. Indeed, Scott et al. (1983) model, modified by Kool and Parker (1987), could generate pumping effects under cyclic pressure variation (Huang et al. 2005; Jaynes 1984; Werner and Lockington 2006). However, with an hCritA value of 10,000 kPa, these effects were minor and did not significantly affect numerical simulations (Bossé 2014). These observations underscore the importance of the hCritA parameter in simulating soil–atmosphere interactions in hysteretic numerical codes used for matric suction prediction. In this study, knowing that the influence of hCritA on the volumetric water content (and the water balance) were relatively minor, the 10,000 kPa value was retained for the numerical simulations to avoid pumping effects.

Conclusions and Recommendations

The influence of hysteresis on the behavior of a 50 cm SR cover with capillary barrier effects in a semi-arid climate was experimentally and numerically investigated. A hydrogeological characterization, including the hysteretic behavior of the SR material, was performed in laboratory instrumented column tests. The transient unsaturated water flow of the SR cover was then predicted using the HYDUS-1D code. A non-hysteretic scenario based on the MWC and a hysteretic scenario were compared. Annual data (year 2011) collected from instrumented field column tests (Bossé et al. 2013) were used to validate these predictions. The main conclusions of this study were:

- Significant hysteretic behavior (hysteretic ratio ≈ 11) of the fine-grained (silty) material used as SR material was measured from laboratory tests.
- Comparisons between field measurements and predicted values of volumetric water content and matric suction time trends showed that the tested numerical model predicted the actual hydrogeological behavior relatively well. The non-hysteretic and hysteretic scenarios correlated better with matric suction field measurements during wet and dry seasons, respectively. Predicted volumetric water contents were relatively similar for both scenarios.
- In the tested semi-arid natural conditions, the water balance components were only slightly affected by scenario type. The hysteretic simulation slightly overestimated the actual evaporation.

This study demonstrated that accounting for hysteresis in numerical simulation of a 50 cm SR cover located in semi-arid climatic conditions can influence predictions of the transient unsaturated water flow. Compared to non-hysteretic predictions, hysteretic predictions suggested better water percolation control. However, the comparison between field and predicted values showed that the hysteretic scenario was less accurate during wet periods, but more representative (in terms of suction changes) during dry seasons. In addition, the hysteretic simulations were more affected by one of the parameters (hCritA) that characterizes soil–atmosphere interactions in the HYDRUS-1D numerical code. For these semi-arid climatic conditions and for this physical field simulation (instrumented column) of an SR cover consisting of a fine-grained material with high hysteretic behavior, the influence of hysteresis effects on the complex transient unsaturated water flow was considered minor. The hysteresis model did not significantly improve predictions. Instead, it predicted a wider range of matric suction values and higher actual evaporation rates than both the non-hysteresis model and field measurements. In practice, for the design of engineered covers in which percolation is the primary concern, preliminary non-hysteretic simulations based on measured or predicted MWCs (e.g. Maqsoud et al. 2012) are recommended for assessing the performance of SR covers and making preliminary predictions of water percolation. Nevertheless, further comparisons between pilot or real-scale field investigations (e.g. Albright et al. 2004; Benson

et al. 2001; Bussière et al. 2007; Nyhan 2005; Scanlon et al. 2005) and hysteretic (WRC and unsaturated hydraulic conductivity functions) numerical predictions are needed to better assess the influence of hysteresis on predictions of the hydrogeological behavior of engineered cover systems under different climatic conditions, and to better determine the relevance of using numerical hysteresis models.

Acknowledgments Financial support was provided under the International Research Chairs Initiative, a program funded by the International Development Research Centre (IDRC) and the Canada Research Chairs Program, and the Industrial NSERC Polytechnique-UQAT Chair on Environment and Mine Wastes Management (Canada).

References

Abbasi F, Javaux M, Vanclooster M, Feyen J (2012) Estimating hysteresis in the soil water retention curve from monolith experiments. Geoderma 189:480–490. doi:10.1016/j.geoderma.2012.06.013

Albright WH, Benson CH, Gee GW, Roesler AC, Abichou T, Apiwantragoon P, Lyles BF, Rock SA (2004) Field water balance of landfill final covers. J Environ Qual 33(6):2317–2332. doi:10.2134/jeq2004.2317

ASTM (2002) D 5856-95: standard test methods for measurement of hydraulic conductivity porous materials using a rigid-wall compaction-mold permeameter. Annu Book ASTM Stand. doi:10.1520/D5856-95R02E01

ASTM (2006) D2434-68: standard test method for permeability of granular soils constant head. Annu Book ASTM Stand. doi:10.1520/D2434-68R06

ASTM (2008) D 6836-02: standard test methods for determination of the soil water characteristic curve for desorption using a hanging column pressure extractor chilled mirror hygrometer and\or centrifuge. Annu Book ASTM Stand. doi:10.1520/D6836-02R08E02

Benson CH (2007) Modeling unsaturated flow and atmospheric interactions. In: Schanz T (ed) Theoretical and numerical unsaturated soil mechanics, vol 113. Springer, Berlin, pp 187–201. doi:10.1007/3-540-69876-0_20

Benson CH, Abichou T, Albright WH, Gee GW, Roesler AC (2001) Field evaluation of alternative earthen final covers. Int J Phytorem 3(1):105–127. doi:10.1080/15226510108500052

Benson CH, Albright WH, Roesler AC, Abichou T (2002) Evaluation of final cover performance: field data from the alternative cover assessment program (ACAP). In: Proceedings of the WM'02 conference, Tucson, AZ, USA. https://www.dri.edu/images/stories/research/programs/acap/acap-publications/8.pdf

Benson CH, Bohnhoff G, Apiwantragoon P, Ogorzalek A, Shackelford C, Albright W (2004) Comparison of model predictions and field data for an ET cover. In: Proceedings of the tailings and mine waste'04, Balkema, Leiden, the Netherlands, pp 137–142

Bohnhoff GL, Ogorzalek AS, Benson CH, Shackelford CD, Apiwantragoon P (2009) Field data and water-balance predictions for a monolithic cover in a semiarid climate. J Geotech Geoenv Eng 135(3):333–348. doi:10.1061/(ASCE)1090-0241

Bossé B (2014) Évaluation du comportement hydrogéologique d'un recouvrement alternatif constitué de rejets calcaires phosphatés en climat semi-aride à aride. PhD Diss, UQAT, Rouyn-Noranda, Canada

Bossé B, Bussière B, Hakkou R, Maqsoud A, Benzaazoua M (2013) Assessment of phosphate limestone wastes as a component of a store-and-release cover in a semiarid climate. Mine Water Environ 32(2):152–167. doi:10.1007/s10230-013-0225-9

Bossé B, Bussière B, Hakkou R, Maqsoud A, Benzaazoua M (2015) Field experimental cells to assess hydrogeological behaviour of store-and-release covers made with phosphate mine waste. Can Geotech J 52:1–15. doi:10.1139/cgj-2014-0263

Bussière B, Aubertin M, Mbonimpa M, Molson JW, Chapuis RP (2007) Field experimental cells to evaluate the hydrogeological behaviour of oxygen barriers made of silty materials. Can Geotech J 44(3):245–265. doi:10.1139/t06-120

Davis DD, Horton R, Heitman JL, Ren TS (2009) Wettability and hysteresis effects on water sorption in relatively dry soil. Soil Sci Soc Am J 73(6):1947–1951. doi:10.2136/sssaj2009.00028N

Decagon (2009) Dielectric water potential sensor. Operator's manual, version 3. Decagon Devices Inc, Pullman

Decagon (2012) EC-5 soil moisture sensor. User's manual, version 1. Decagon Devices Inc, Pullman

Dwyer SF (2003) Water balance measurements and computer simulations of landfill covers. PhD Diss, Univ of New Mexico, Albuquerque, NM, USA

Fala O, Molson J, Aubertin M, Bussière B (2005) Numerical modeling of flow and capillary barrier effects in unsaturated wastes rock piles. Mine Water Environ 24(4):172–185. doi:10.1007/s10230-005-0093-z

Fayer MJ, Gee GW (1997) Hydrologic model tests for landfill covers using field data. In: Proceedings of the landfill capping in the semi-arid west: problems, perspectives and solutions. Env Sci and Res Foundation, Idaho Falls, ID, USA, pp 53–68

Fayer MJ, Rockhold ML, Campbell MD (1992) Hydrologic modeling of protective barriers: comparison of field data and simulation results. Soil Sci Soc Am J 56(3):690–700. doi:10.2136/sssaj1992.03615995005600030004x

Fredlund DG, Rahardjo H (1993) Soil mechanics for unsaturated soils. Wiley, New York

Fredlund DG, Xing A (1994) Equations for the soil-water characteristic curve. Can Geotech J 31(4):521–532. doi:10.1139/t94-061

Haines WB (1930) Studies in the physical properties of soil. V. The hysteresis effect in capillary properties, and the modes of moisture distribution associated therewith. J Agric Sci 20(1):97–116. doi:10.1017/S002185960008864X

Haverkamp R, Reggiani P, Ross PJ, Parlange JY (2002) Soil water hysteresis prediction model based on theory and geometric scaling. Environ Mech Water Mass Energy Transf Biosph Philip 129:213–246. doi:10.1029/129GM19

Hogarth W, Hopmans J, Parlange JY (1988) Applications of a simple soil water hysteresis model. J Hydrol 98(1):21–29. doi:10.1016/0022-1694(88)90203-X

Huang HC, Tan YC, Liu CW, Chen CH (2005) A novel hysteresis model in unsaturated soil. Hydrol Proc 19(8):1653–1665. doi:10.1002/hyp.5594

Huang M, Barbour SL, Elshorbagy A, Zettl JD, Si BC (2011) Infiltration and drainage processes in multi-layered coarse soils. Can J Soil Sci 91(2):169–183. doi:10.4141/CJSS09118

Huang M, Bruch PG, Barbour SL (2013) Evaporation and water redistribution in layered unsaturated soil profiles. Vadose Zone J 12(1). doi:10.2136/vzj2012.0108

Jaynes DB (1984) Comparison of soil-water hysteresis models. J Hydrol 75(1):287–299. doi:10.1016/0022-1694(84)90054-4

Khire MV, Benson CH, Bosscher PJ (1997) Water balance modeling of earthen final covers. J Geotech Geoenv Eng 123(8):744–754. doi:10.1061/(ASCE)1090-0241

Khire MV, Benson CH, Bosscher PJ (1999) Field data from a capillary barrier and model predictions with UNSAT-H. J Geotech Geoenv Eng 125(6):518–527. doi:10.1061/(ASCE)1090-0241

Khire MV, Benson CH, Bosscher PJ (2000) Capillary barriers: design variables and water balance. J Geotech Geoenv Eng 126(8):695–708. doi:10.1061/(ASCE)1090-0241

Kool JB, Parker JC (1987) Development and evaluation of closed-form expressions for hysteretic soil hydraulic properties. Water Resour Res 23(1):105–114. doi:10.1029/WR023i001p00105

Lee KS (2007) Effects of hysteresis in k–S–p relationship on the performance of mine waste soil covers. Geosc J 11(3):241–247. doi:10.1007/BF02913937

Li XS (2005) Modeling of hysteresis response for arbitrary wetting/drying paths. Comput Geotech 32(2):133–137. doi:10.1016/j.compgeo.2004.12.002

Liu Y, Parlange JY, Steenhuis TS, Haverkamp R (1995) A soil water hysteresis model for fingered flow data. Water Resour Res 31(9):2263–2266. doi:10.1029/95WR01649

Maqsoud A, Bussière B, Aubertin M, Mbonimpa M (2012) Predicting hysteresis of the water retention curve from basic properties of granular soils. Geotech Geol Eng 30(5):1147–1159. doi:10.1007/s10706-012-9529-y

McCarthy DF (2007) Essentials of soil mechanics and foundations: basic geotechnics, 7th edn. Prentice Hall, Upper Saddle River

Miller EE, Miller RD (1956) Physical theory for capillary flow phenomena. J Appl Phys 27(4):324–332. doi:10.1063/1.1722370

Mitchell RJ, Mayer AS (1998) The significance of hysteresis in modeling solute transport in unsaturated porous media. Soil Sci Soc Am J 62(6):1506–1512. doi:10.2136/sssaj1998.03615995006200060005x

Morris CE, Stormont JC (1997) Capillary barriers and subtitle D covers: estimating equivalency. J Environ Eng 123(1):3–10. doi:10.1061/(ASCE)0733-9372

Morris CE, Stormont JC (1998) Evaluation of numerical simulations of capillary barrier field tests. Geotech Geol Eng 16(3):201–213. doi:10.1023/A:1008853710339

Mualem Y (1974) A conceptual model of hysteresis. Water Resour Res 10(3):514–520. doi:10.1029/WR010i003p00514

Mualem Y (1977) Extension of the similarity hypothesis used for modeling the soil water characteristics. Water Resour Res 13(4):773–780. doi:10.1029/WR013i004p00773

Mualem Y (1984a) Prediction of the soil boundary wetting curve. J Soil Sci 137(6):379–390. doi:10.1097/00010694-198406000-00001

Mualem Y (1984b) A modified dependent domain theory of hysteresis. J Soil Sci 137(5):283–291. doi:10.1097/00010694-198405000-00001

Mualem Y, Beriozkin A (2009) General scaling rules of the hysteretic water retention function based on Mualem's domain theory. Eur J Soil Sci 60(4):652–661. doi:10.1111/j.1365-2389.2009.01130.x

Nimmo JR (1992) Semi-empirical model of soil water hysteresis. Soil Sci Soc Am J 56:1723–1730. doi:10.2136/sssaj1992.03615995005600060011x

Nuth M, Laloui L (2008) Advances in modeling hysteretic water retention curve in deformable soils. Comput Geotech 35(6):835–844. doi:10.1016/j.compgeo.2008.08.001

Nyhan JW (2005) Seven-year water balance study of an evapotranspiration landfill cover varying in slope for semiarid regions. Vadose Zone J 4(3):466–480. doi:10.2136/vzj2003.0159

Ogan BD, Wilson GV, Albright WH, Gee GW, Fayer MJ, Rock S (1999) Sensitivity analysis and validation of numerical models used in the design of alternative landfill covers. Annual Meeting Abstracts, Soil Sci Soc of Am, Salt Lake City, UT, USA

Ogorzalek AS, Bohnhoff GL, Shackelford CD, Benson CH, Apiwantragroon P (2008) Comparison of field data and water-balance predictions for a capillary barrier cover. J Geotech Geoenv Eng 134(4):470–486. doi:10.1061/(ASCE)1090-0241

Pang L, Close ME, Watt JPC, Vincent KW (2000) Simulation of picloram atrazine and simazine leaching through two New Zealand soils and into groundwater using HYDRUS-2D. J Cont Hydrol 44(1):19–46. doi:10.1016/S0169-7722(00)00091-7

Parker JC, Lenhard RJ (1987) A model for hysteretic constitutive relations governing multiphase flow. 1 saturation—pressure relations. Water Resour Res 23(12):2187–2196. doi:10.1029/WR023i012p02187

Parlange JY (1976) Capillary hysteresis and the relationship between drying and wetting curves. Water Resour Res 12(2):224–228. doi:10.1029/WR012i002p00224

Pedroso DM, Williams DJ (2010) A novel approach for modeling soil water retention characteristic curves with hysteresis. Comput Geotech 37(3):374–380. doi:10.1016/j.compgeo.2009.12.004

Pham QH, Fredlund DG, Barbour SL (2003) A practical hysteresis model for the soil-water characteristic curve for soils with negligible volume change. Géotechnique 53(2):293–298. doi:10.1680/geot.2003.53.2.293

Poulovassilis A (1962) Hysteresis of pore water an application of concept of independent domains. Soil Sci 93(6):405–412. doi:10.1097/00010694-196206000-00007

Richards LA (1931) Capillary conduction of liquids through porous mediums. Physics 1:318–333. doi:10.1063/1.1745010

Rock S, Myers B, Fiedler L (2012) Evapotranspiration (ET) Covers. Int J Phytoremediat 14(S1):1–25. doi:10.1080/15226514.2011.609195

Royer JM, Vachaud G (1975) Field determination of hysteresis in soil-water characteristic. Soil Sci Soc Am J 39(2):221–223. doi:10.2136/sssaj1975.03615995003900020006x

Scanlon BR, Christman M, Reedy RC, Porro I, Šimůnek J, Flerchinger GN (2002) Intercode comparisons for simulating water balance of surficial sediments in semiarid regions. Water Resour Res 38(12):1323–1339. doi:10.1029/2001WR001233

Scanlon BR, Reedy RC, Keese KE, Dwyer SF (2005) Evaluation of evapotranspirative covers for waste containment in arid and semiarid regions in the southwestern USA. Vadose Zone J 4(1):55–71. doi:10.2136/vzj2005.0055

Schaap MG, Leij FJ (2000) Improved prediction of unsaturated hydraulic conductivity with the Mualem-van Genuchten model. Soil Sci Soc Am J 64(3):843–851. doi:10.2136/sssaj2000.643843x

Scott PS, Farquhar GJ, Kouwen N (1983) Hysteretic effects on net infiltration. Advances in infiltration. Am Soc of Agri Eng, Chicago, pp 163–170

Shackelford CD, Chang CK, Chiu TF (1994) The capillary barrier effect in unsaturated flow through soil barriers. In: Proceedings of the 1st international congress on Env Geotech, Edmonton, Canada, pp 789–793

Si BC, Kachanoski RG (2000) Unified solution for infiltration and drainage with hysteresis: theory and field test. Soil Sci Soc Am J 64(1):30–36. doi:10.2136/sssaj2000.64130x

Šimůnek J, Kodešová R, Gribb MM, van Genuchten MTh (1999) Estimating hysteresis in the soil water retention function from cone permeameter experiments. Water Resour Res 35(5):1329–1345. doi:10.1029/1998WR900110

Šimůnek J, van Genuchten MTh, Šejna M (2008) Development and applications of the HYDRUS and STANMOD software packages and related codes. Vadose Zone J 7(2):587–600. doi:10.2136/vzj2007.0077

Šimůnek J, Šejna M, Saito H, Sakai M, van Genuchten MTh (2009) The HYDRUS-1D software package for simulating the one-dimensional movement of water heat and multiple solutes in variability-saturated media. Version 415, Dept of Env Sci, Univ of California, Riverside, CA, USA

Stormont JC, Anderson C (1999) Capillary barrier effect from underlying coarser layer. J Geotech Geoenv Eng 125(8):641–648. doi:10.1061/(ASCE)1090-0241

Stormont JC, Morris CE (1998) Method to estimate water storage capacity of capillary barriers. J Geotech Geoenv Eng 124(4):297–302. doi:10.1061/(ASCE)1090-0241

Tan YC, Ma KC, Chen CH, Ke KY, Wang MT (2009) A numerical model of infiltration processes for hysteretic flow coupled with mass conservation. Irrig Drain 58(3):366–380. doi:10.1002/ird.403

Topp GC (1971) Soil-water hysteresis: the domain theory extended to pore interaction conditions. Soil Sci Soc Am J 35(2):219–225. doi:10.2136/sssaj1971.03615995003500020017x

Van Genuchten MTh (1980) A closed form equation for predicting the hydraulic conductivity of unsaturated soils. Soil Sci Soc Am J 44:892–898. doi:10.2136/sssaj1980.03615995004400050002x

Vereecken H, Diels J, Viaene P (1995) The effects of soil heterogeneity hysteresis on solute transport: a numerical experiment. Ecoll Model 77:273–288. doi:10.1016/0304-3800(94)00183-I

Vogel TK, Huang K, Zhang R, van Genuchten MTh (1996) The HYDRUS code for simulating one-dimensional water flow solute transport and heat movement in variably-saturated media. Version 5, research report 140, US Salinity Laboratory, USDA ARS, Riverside, CA, USA

Watson KK, Reginato RJ, Jackson RD (1975) Soil water hysteresis in a field soil. Soil Sci Soc Am J 39(2):242–246. doi:10.2136/sssaj1975.03615995003900020010x

Werner AD, Lockington DA (2006) Artificial pumping errors in the Kool-Parker scaling model of soil moisture hysteresis. J Hydrol 325:118–133. doi:10.1016/j.jhydrol.2005.10.012

Wilson GW, Fredlund DG, Barbour SL (1997) The effect of soil suction on evaporative fluxes from soil surfaces. Can Geotech J 34(1):145–155. doi:10.1139/t96-078

Yang H, Rahardjo H, Wibawa B, Leong EC (2004) A soil column apparatus for laboratory infiltration study. Geotech Test J 27(4):347–355. doi:10.1520/GTJ11549

Yang C, Sheng D, Carter JP (2012a) Effect on hydraulic hysteresis on seepage analysis for unsaturated soils. Comput Geotech 41:36–56. doi:10.1016/j.compgeo.2011.11.006

Yang C, Sheng D, Carter JP (2012b) Stochastic evaluation of hydraulic hysteresis in unsaturated soils. J Geotech Geonenviron Eng 39(7):1211–1214. doi:10.1061/(ASCE)GT.1943-5606.0000833

Zhan G, Keller J, Milczarek M, Giraudo J (2014) 11 years of evapotranspiration cover performance at the AA leach pad at Barrick Goldstrike Mines. Mine Water Environ 33(3):195–205. doi:10.1007/s10230-014-0268-6

Zhang Q, Werner AD, Aviyanto RF, Hutson JL (2009) Influence of soil moisture hysteresis on the functioning of capillary barriers. Hydrol Process 23(9):1369–1375. doi:10.1002/hyp.7261

Zhou AN (2013) A contact angle-dependent hysteresis model for soil-water retention behavior. Comput Geotech 49:36–42. doi:10.1016/j.compgeo.2012.10.004